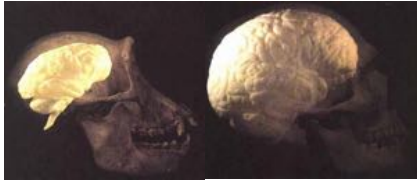


Brain Evolution



Introduction to Anthropogeny

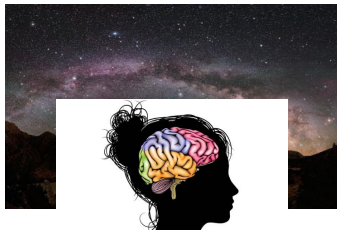
Lecture 4

Pascal Gagneux

October 19, 2023

The Human Brain a galaxy of its own

100 billion stars in the milky way,
more cells in your brain!



86 billion neurons and 85 billion non-neurons

The Human Brain in Numbers: A Linearly Scaled-up Primate Brain
Suzana Herculano-Houzel 2009 *Front Hum Neurosci.* 3: 31.

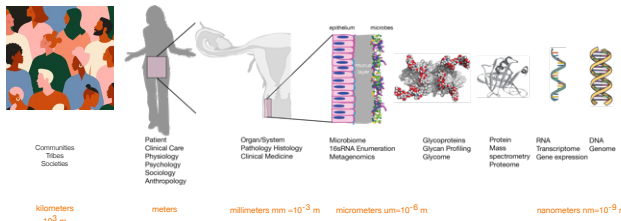
100 billion stars in the milky way, more cells in your brain!

Practice question: Why is the human brain regularly compared to our galaxy?

Answer: Similar number of cells as stars in the galaxy.

Scales: Societies to Atoms....

What scale are we considering?

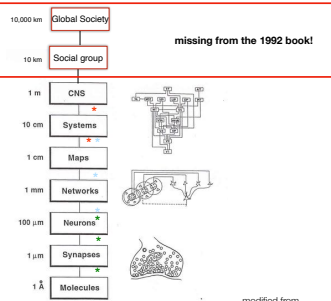


Our molecular nature ranges from atoms to societies.

Scales of investigation

How do we study the composition of the brain non-invasively in humans & apes?

- Imaging of living brain (MRIs, DTIs, PET)
- Histology of brain after organ donation
- IPS cells
 - mRNA
 - RNA binding protein
 - mRNA



modified from Sejnowski & Churchland 1992

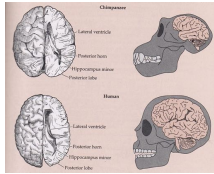
Human Central nervous systems develop embedded in societies, cultural input is crucially important for neuro-typical development

The search for human-specific brain structures

Owen-Huxley Debate



Richard Owen standing next to the skeleton of an extinct moa bird of New Zealand.



Thomas Henry Huxley (1825-1895) - "Darwin's Bulldog"

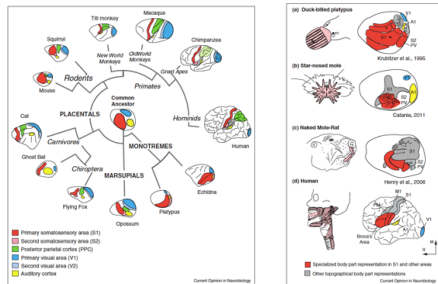


"hippocampus minor" now calcar avis: the ridge running along the floor of the temporal horn of the lateral ventricle

Claims for uniquely human brain features have a long tradition, but require rigorous comparisons.

Cortical area and ecological function

Size of a neural region is related to its functional significance in mammals



Krubitzer & Stoilzenberg 2013

The mammalian cortex can devote different amounts of real estate to particularly relevant features.

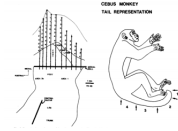
By the Tail!



Muriqui, an atelid monkey of Brazil



Capuchin, a cebid monkey of S. America

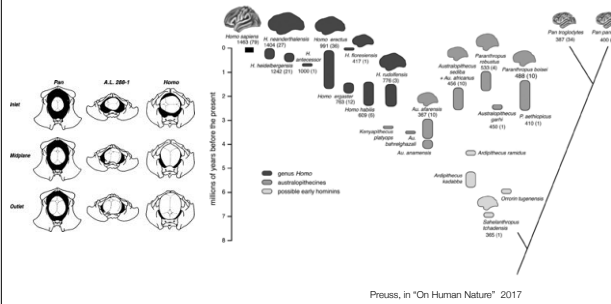


Felleman et al., J Brain Science 1983

Your brain reflects your body parts and how you use them in both Nature and Culture!

Prehensile tails evolved twice, independently into groups of New World Primates. Their brains devote a substantial part of their cortical “real estate” to control of the tails and sensory detection via the “fingerprint” like pad on the underside of the tail.

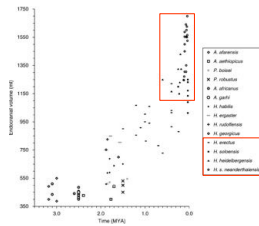
The fossil record of hominin phylogeny and brain size evolution



The fossil record of hominin phylogeny and brain size evolution. Date ranges for fossils are from Wood and Baker (2011). Brain sizes (in cubic centimeters) are from de Sousa and Cunha (2012) and, for *Pan paniscus* only, from Hopkins et al. (2009). Sample sizes are indicated in parentheses. Wood and Baker are not explicit about the details of relationships among each of the species, but there is general agreement that the genus *Homo* evolved from an australopithecine ancestor.

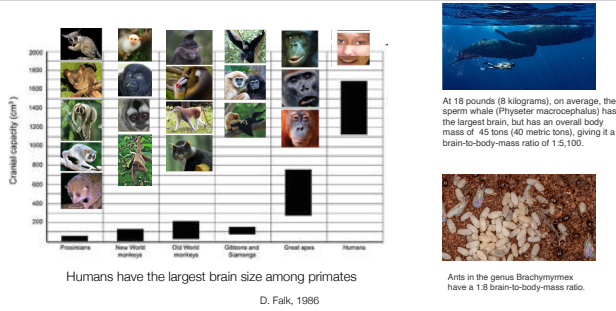
Brain Size in Evolutionary Time

Perfectly normal and functional human brains vary by 1 kg!!

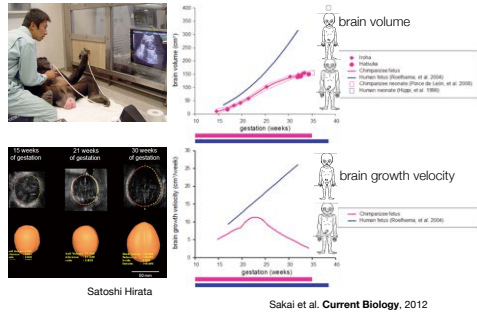


Several extinct hominins fit well within modern human brain size variation

Absolute Brain Size



How to grow a big brain

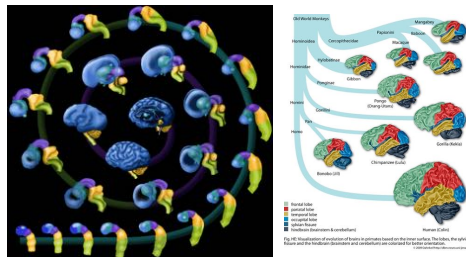


Gestational age-related changes in brain volume in chimpanzee (Hatsuka and Iroha) and human fetuses.

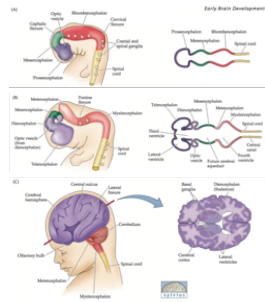
Gestational age-related changes in the growth velocity of brain volume in chimpanzee and human fetuses

Chimpanzee brains start slowing down their growth in mid-pregnancy, humans on the other hand continue a high fetal rate for a full year after birth.

Brain development: from tube to walnut

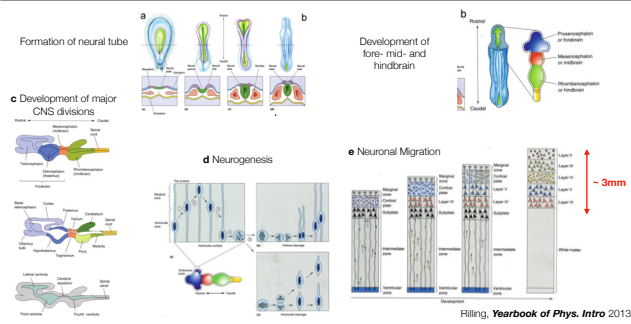


Brain development more views:



Much of the hollow space under the cortex (with a thickness of 1 to 7mm, average in humans 2.5mm) becomes filled with connections (white matter)

Thin walled tube to six-layer cortex

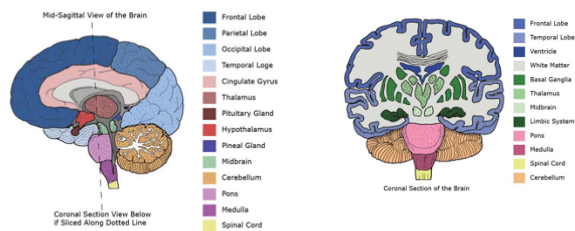


Mechanisms of neurodevelopment.

- (a) Formation of the neural tube,
- (b) development of forebrain, midbrain, and hindbrain vesicles,
- (c) development of major CNS divisions,
- (d) neurogenesis,
- (e) neuronal migration. [Reprinted from Bear MF et al.2001. Neuroscience: Exploring the Brain. Pages 179–711. C 2001

A rough map

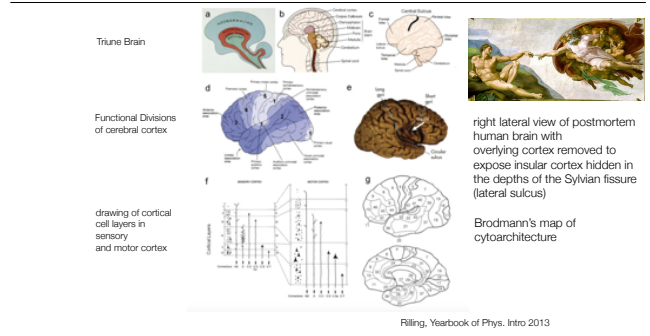
Cross Section Images of the Brain



<https://www.healthpages.org/anatomy-function/brain-anatomy/>

Anatomist have coined distinct names for distinct regions of the cortex and subcortical regions of the brain.

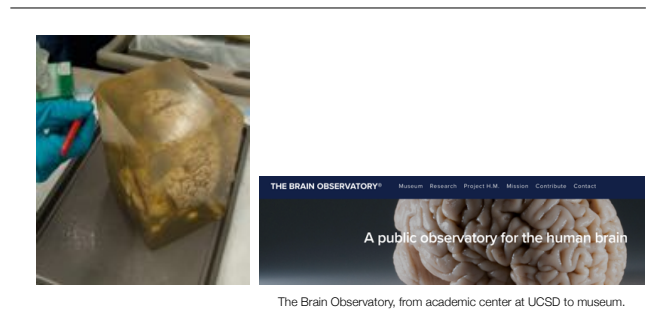
Overview of the human central nervous system



Overview of the human central nervous system.

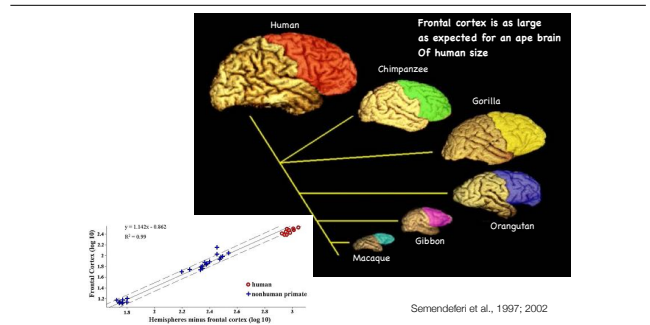
- (a) Triune brain model,
- (b) seven main divisions of central nervous system,
- (c) lateral view of the human brain
- (d) functional divisions of cerebral cortex, 1 5 primary sensory and motor cortex, 2 5 association cortex, 3 5 prefrontal cortex, 4 5 premotor cortex, 5 5 primary motor cortex,
- (e) right lateral view of postmortem human brain with overlying cortex removed to expose insular cortex hidden in the depths of the Sylvian fissure,
- (f) drawing of cortical cell layers in sensory and motor cortex,
- (g) Brodmann's cytoarchitectonic map of the human cerebral cortex,

Brain Slices

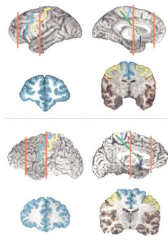


Jacopo Annese, Ph D.

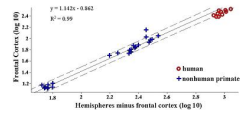
Relative Size of Frontal Cortex



Anatomically informed boundaries show that..



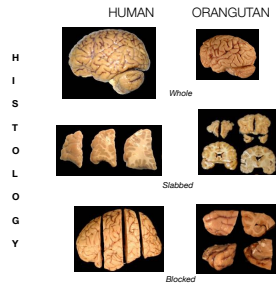
The human frontal cortex, both a) with and b) without the precentral gyrus (primary motor cortex) is as large as expected for an ape of human brain size



Semendefeni et al., 1997; 2002

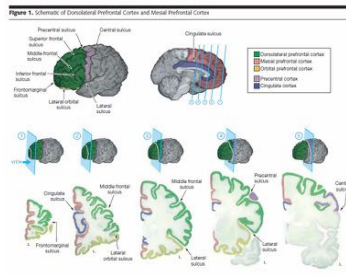
Quantitative, Cellular & Molecular Analyses

Cytoarchitecture
Myeloarchitecture
Chemoarchitecture
Gene expression/Molecular:
"Geschwind & Rakic, *Neuron* 2013"



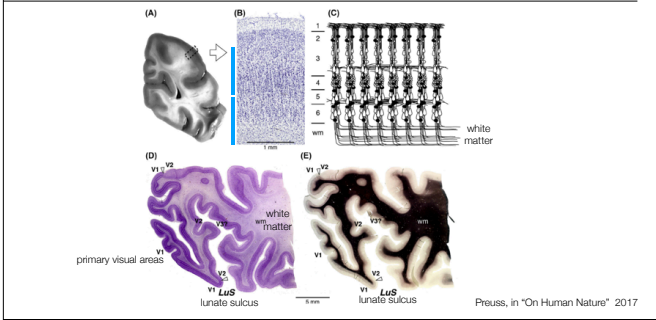
Brain Anatomy

Defining and using Anatomical Boundaries



Schematics of 2 prefrontal subregions, dorsolateral prefrontal cortex (green) and medial prefrontal cortex (orange). Within each region, neuron counts, neuron size, and glia counts were performed using unbiased stereological methods.

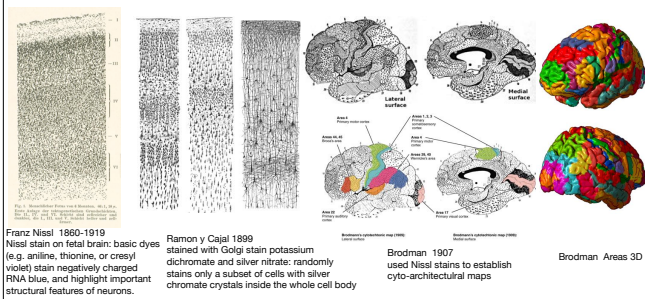
Laminar, columnar, and areal organization of cerebral cortex



Laminar, columnar, and areal organization of cerebral cortex.

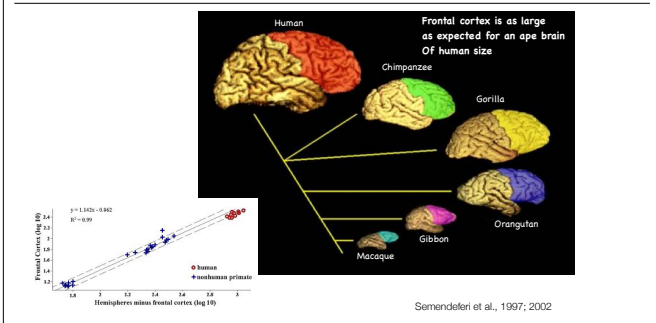
- (A) An unstained section through the posterior right cerebral hemisphere of a human; the inset shows the small region of gray matter illustrated at higher magnification in B.
- (B) A section of cortical gray matter stained for Nissl substance to illustrate the six tangential layers and the vertically oriented minicolumns. In this section, the columnar appearance of the cortex is most obvious in layers 4 and 5.
- (C) A schematic representation of cortical microstructure, showing the vertical clustering of neurons and the predominantly vertical, intracolumnar organization of intrinsic (local) connections, although some layers also have prominent horizontal, intralaminar connections as well. Most long connections travel in the white matter (wm). Collections of continuous minicolumns, with similar connections and cellular organization, make up the areas, the next higher-order unit. (
- (D, E) Low-magnification view of a horizontal section through the posterior right hemisphere of an orangutan, stained for Nissl (D) and myelin
- (E) to illustrate cyto- and myeloarchitectonic differences between cortical areas. Posterior is to the left, lateral to the bottom. In both stains, the distinctive, highly laminated character of the primary visual area (V1) is apparent, and the border between V1 and the second visual area (V2), marked with arrowheads, is easily identified. Laterally, the border is close to the lip of the lunate sulcus (LuS, a deep fissure in apes and macaques, but absent in monkeys). While the other cortex in these sections is not homogeneous in Nissl or myelin, distinct borders, such as that between V2 and V3, which presumably occupies the anterior bank of the LuS, are often difficult

Korbinian Brodman (1868-1918) and brain cytoarchitecture

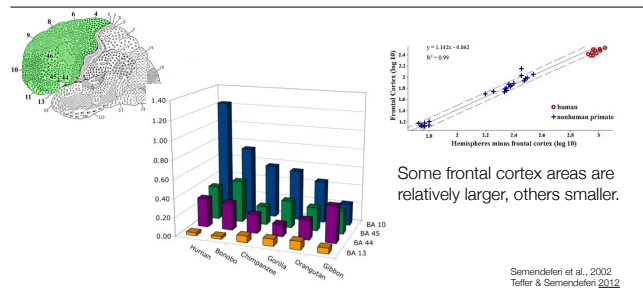


The Nissl stain shows the cell bodies of neurons on the right in a 6 month old human fetus
Golgi stain shows the dendrites and axons of a random subset of neurons.

Relative Size of Frontal Cortex



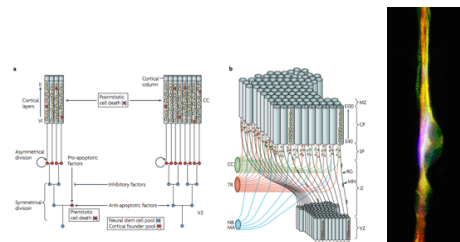
The relative size distribution of areas within the frontal lobe differs between apes & humans



Pre-adapted brains?



Radial unit lineage model of cortical neurogenesis



Rakic, P 2009 *Nature Rev Neurosciences*

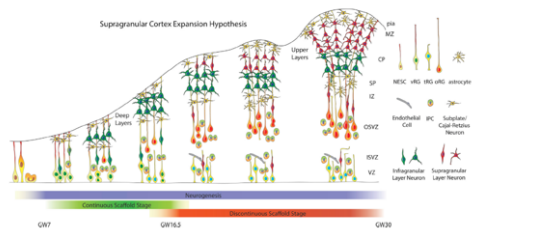
Radial unit lineage model of cortical neurogenesis. a | Based on the radial unit hypothesis^{12,30}, the model illustrates how changes in the mode and the rates of cell proliferation and/or programmed cell death within the neural stem cell pool (blue circles) in the ventricular zone (VZ) that divide symmetrically at early embryonic stages causes an exponential increase in the number of radial columns, which, in turn, results in surface expansion of the cerebral cortex without changes in its thickness. By contrast, similar changes in proliferation kinetics occurring in the founder cells (red circles), which divide asymmetrically, cause a linear increase in the number of neurons within radial columns without a change in the cortical surface area. b | The model of radial neuronal migration that underlies columnar organization. The cohorts of neurons generated in the VZ traverse the intermediate zone (IZ) and subplate zone (SP) containing 'waiting' afferents from several sources (cortico-cortical connections (CC), thalamic radiation (TR), nucleus basalis (NB), monoamine subcortical centers (MA)) and finally pass through the earlier generated deep layers before settling in at the interface between the cortical plate (CP) and marginal zone (MZ). The timing of neurogenesis (E40–E100) refers to the embryonic age in the macaque monkey. The positional information of the neurons in the VZ and corresponding protomap within the SP and CP is preserved during cortical expansion by transient radial glial scaffolding. Further details can be viewed in the Rakic laboratory animated video of radial migration. RG, radial glia cell; MN, migrating neuron.

Vertical Organization of the cortex



Like a pygmy man climbing a giant tree to find honey, neurons from the subventricular zone climb along radial glial cells during cortical development.

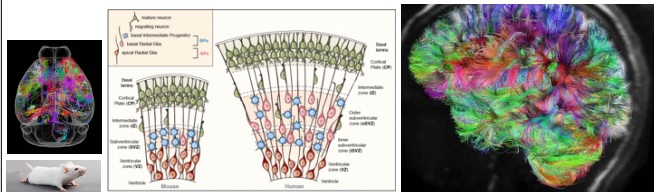
Cortical Neurogenesis in two phases?



Nowakowski et al. *Neuron* 2016, Kriegstein Lab UCSF

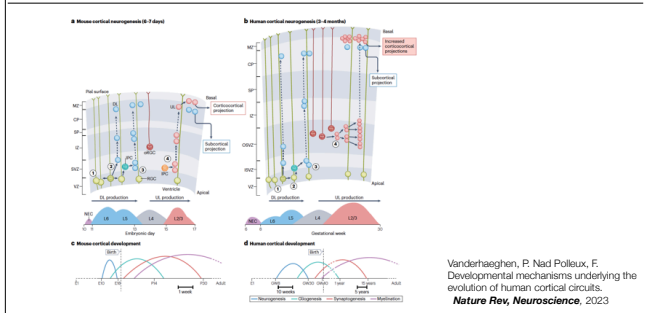
The Supragranular Cortex Expansion Hypothesis: By integrating experimental evidence in the published literature with our experimental findings, we propose that primate cortical neurogenesis can be divided into two stages. During early neurogenesis (left), basal fibers of ventricular radial glia contact the pial surface and newborn neurons migrate along ventricular as well as outer radial glia fibers. During late neurogenesis (right), newborn neurons reach the cortical plate only along outer radial glia fibers. VZ, ventricular zone; NESC, neuroepithelial stem cell; ISVZ, inner subventricular zone; OSVZ, outer subventricular zone; IZ, intermediate zone; SP, subplate; CP, cortical plate; MZ, marginal zone; IPC, intermediate progenitor cell; vRG, ventricular radial glia; tRG, truncated radial glia; oRG, outer radial glia.

Mouse Model?



Cartoon illustrating apical Radial Glia (APs) and Basal Radial Glia (BPs) in embryonic mouse and fetal human neocortex. Mouse is left, human is right. Note the increase in BPs and the expansion of the SVZ in fetal human neocortex.

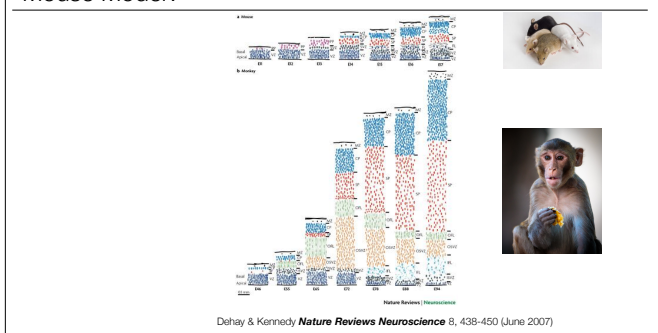
Delay of cortical synaptic development



Age-related gene expression change in the PFC and CBC. (A) Age distribution of samples used in this study. Each point represents an individual, with technical replicates shown as a second point below the first. Only one of the two replicates was used in the main analysis. The colors indicate brain regions (red, PFC; gray, CBC). The x-axis represents individual age in fourth root (age^{1/4}) scale. The numbers of age-related genes (B) and genes with species-specific expression profiles (C) identified in the PFC (red) or CBC (gray). The red arrows highlight excess human-specific expression changes in the PFC.

Synaptic density changes during human, chimpanzee, and macaque PFC development. (A) Example of synapses viewed by electron microscopy (red arrows), in the PFC of a 32-d-old chimpanzee. (B) Mean synaptic density per 100 mm² measured in the PFC of humans (red), chimpanzees (blue), and rhesus macaques (green) at different ages. (Error bars) 95% confidence intervals obtained by bootstrapping synaptic density values within samples 1000 times. Independent assessment of synaptic density by another investigator is plotted on Supplemental The phylogenetic relationship of human, Neanderthal, chimpanzee, and rhesus macaque species. (Red arrow) Human lineage. The numbers show approximate divergence time in millions of years (Kumar and Hedges 1998; Pa^abo 1999; Chen and Li 2001). (B) Proportion of human-derived SNPs measured using a 50-kb sliding window in the MEF2A gene region (red). SNPs were classified as derived according to the method described by Green et al. (2010). (Gray dashed line) Genome average. (Red arrow) Location, upstream of MEF2A, with significant excess of human-derived SNPs (one-sided Fisher's exact test, P = 0.00006). (C) Distribution of the proportion of human-derived SNPs for all windows across the human genome. (Red arrow) Probability of finding the observed proportion of human-derived SNPs in the location 50–100 kb upstream of MEF2A, estimated from the genome distribution.

Mouse Model?

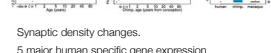
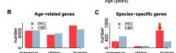
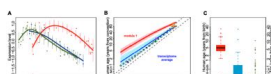
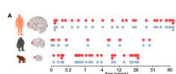


Dramatic differences in size and cellular architecture between mouse and human cortex.

Delay of cortical synaptic development

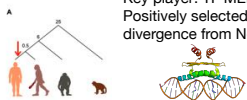
Gene expression in two cortical areas of chimpanzees, humans and monkeys

Time shift in expression of "module 1" genes



Synaptic density changes.
5 major human specific gene expression modules found in PFC.

Key player: TF MEF2A:
Positively selected since divergence from Neanderthal

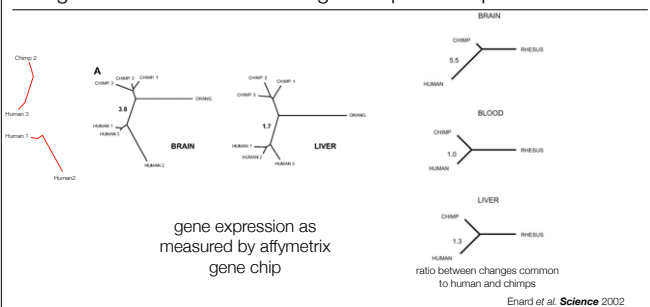


Liu et al. *Genome Research*, 2012
Phillip Khaitovich

Age-related gene expression change in the PFC and CBC. (A) Age distribution of samples used in this study. Each point represents an individual, with technical replicates shown as a second point below the first. Only one of the two replicates was used in the main analysis. The colors indicate brain regions (red, PFC; gray, CBC). The x-axis represents individual age in fourth root (age^{1/4}) scale. Numbers of age-related genes (B) and genes with species-specific expression profiles (C) identified in the PFC (red) or CBC (gray). The red arrows highlight excess human-specific expression changes in the PFC.

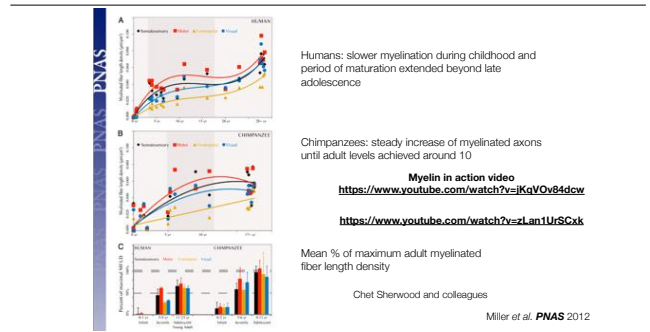
Synaptic density changes during human, chimpanzee, and macaque PFC development. (A) Example of synapses viewed by electron microscopy (red arrows), in the PFC of a 32-d-old chimpanzee. (B) Mean synaptic density per 100 mm² measured in the PFC of humans (red), chimpanzees (blue), and rhesus macaques (green) at different ages. (Error bars) 95% confidence intervals obtained by bootstrapping synaptic density values within samples 1000 times. Independent assessment of synaptic density by another investigator is plotted on Supplemental The phylogenetic relationship of human, Neanderthal, chimpanzee, and rhesus macaque species. (Red arrow) Human lineage. The numbers show approximate divergence time in millions of years (Kumar and Hedges 1998; Pa^abo 1999; Chen and Li 2001). (B) Proportion of human-derived SNPs measured using a 50-kb sliding window in the MEF2A gene region (red). SNPs were classified as derived according to the method described by Green et al. (2010). (Gray dashed line) Genome average. (Red arrow) Location, upstream of MEF2A, with significant excess of human-derived SNPs (one-sided Fisher's exact test, P = 0.00006). (C) Distribution of the proportion of human-derived SNPs for all windows across the human genome. (Red arrow) Probability of finding the observed proportion of human-derived SNPs in the location 50–100 kb upstream of MEF2A, estimated from the genome distribution.

Distance trees representing the relative extent of expression changes in brain and liver among three primate species



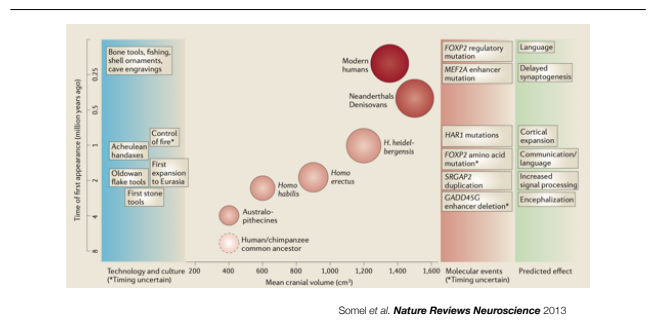
Distance trees representing the relative extent of expression changes in brain and liver among three primate species. Individual humans can have gene expression differences in the cortex that are almost as large as that between a human and a chimpanzee!

Prolonged myelination in human neocortical evolution



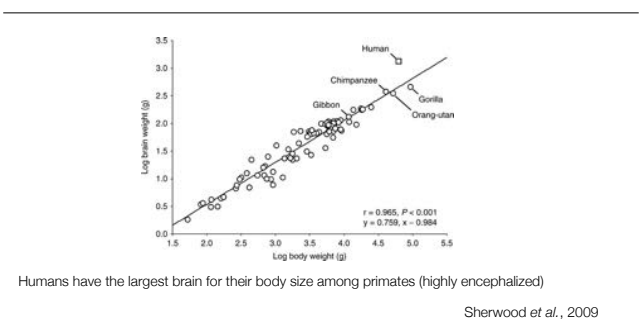
Developmental trajectory of myelinated fiber length density (MFLD). Graphs show best-fit curves for MFLD data in humans (A; n=24) and chimpanzees (B; n=20) arranged by age in years. The shaded vertical area represents time between weaning and full sexual maturation. Diamonds represent somatosensory area (area 3b), squares represent motor area (area 4), triangles represent frontopolar area (area 10), and circles represent visual area (area 18). (C) Bar graph depicts mean percent of maximum mature adult MFLD across development in humans (Left) and chimpanzees (Right). Error bars represent SEM. The thin and thick horizontal dashed lines represent 50% and 100%, respectively, of maximum MFLD. Black represents somatosensory area (area 3b), red represents motor area (area 4), gold represents frontopolar area (area 10), and blue represents visual area (area 18).

Brain expansion over time

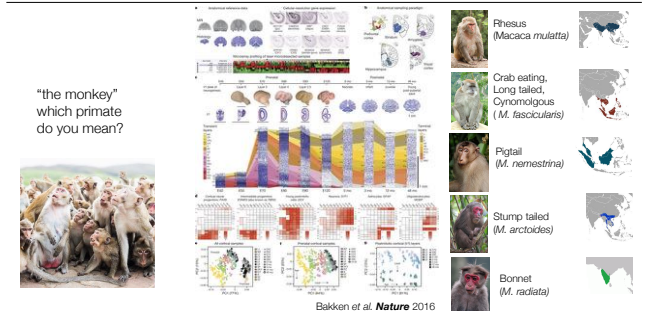


Anatomical differences between human and chimpanzee brains, changes in cranial size in the human fossil record, and archaeological records of tools and cultural artefacts together present a general picture of the evolutionary steps that have led to the emergence of the human brain and cognitive abilities. From the most recent common ancestor of humans and chimpanzees 6–8 million years ago (mya) until the dawn of the genus *Homo* approximately 2.5 mya, all early human ancestors had ape-like cranial volumes. By contrast, subsequent *Homo* species had both higher absolute cranial capacities and higher cranium-to-body ratios (also known as encephalization quotients). For example, the early *Homo habilis* (2.3–1.6 mya) had a cranium that was 1.5 times larger than that of modern chimpanzees. *Homo erectus*, a hominid species that populated our planet between 1.9 mya and 200 thousand years ago (kya), had a cranium that was initially twice as large. *Homo heidelbergensis*, another hominid ancestor that appeared approximately 1 mya, had a cranial capacity approximately three times that of modern chimpanzees, overlapping with that of modern humans (*Homo sapiens sapiens*, 200 kya/149), whereas Neanderthals (*Homo sapiens neanderthalis*, from 400–800 kya to 30 kya/35, 39) evolved cranial sizes that surpassed those of modern humans. Compared to ancestral hominins, increased cranial capacity probably augmented the general and social intelligence of *Homo* species. Encephalization might have been the basis for the Oldowans (2.6–1.4 mya) and Acheulean (1.8–0.25 mya) stone tool technologies, and could have set the ground for the first out-of-Africa hominid colonizations undertaken by *Homo erectus*. Tool use for scavenging, hunting and digging tubers, and the subsequent control of fire and invention of cooking are thought to have promoted human encephalization by enriching nutritional content and increasing energy input. Technological advance, access to high-quality food and encephalization thus appear to have evolved hand-in-hand. However, exceptions to this concept of parallel evolution might exist, such as the not yet fully understood case of the small-brained *Homo floresiensis* species, who used stone tools but had an ape-like cranial volume. Recent comparative genomic studies have identified a number of mutations in the modern human genome that could underlie the evolution of larger brain size and behavioural traits. In agreement with the fossil record, these mutations are shared with extinct hominid species, indicating that encephalization and certain behavioural changes evolved early in the evolution of *Homo*. For example, a deletion of one enhancer of the growth arrest and DNA-damage-inducible gamma (*GADD45G*) gene, which is postulated to have led to brain size expansion, is shared with Neanderthals. Likewise, a human-specific duplication of a truncated version of the gene *SLIT-ROBO Rho GTPase activating protein 2* (*SRGAP2*) was dated to approximately 2.4 mya. This duplication is predicted to increase dendritic spine density in the cortex and could have enhanced signal processing in the hominid brains (see the figure). It is also worth noting that both Neanderthals and Denisovans — the two extinct hominid species that diverged from the human evolutionary lineage 400–800 kya differ from other primates by the same two amino acid changes as modern humans in the gene encoding forkhead box P2 (*FOXP2*). As these amino acid substitutions have been linked to the evolution of human language and changes in brain connectivity, it is conceivable that Neanderthals and Denisovans also possessed certain types of human-like linguistic abilities. Remarkably, although the late *Homo* species showed an increase in brain size to and beyond that of modern humans, their Acheulean technology (1.8–0.25 mya), mainly consisting of stone flakes and hand-axes, made only limited progress for nearly 1.5 million years. This cultural and technological standstill contrasts with the rapid cultural explosion observed in the archaeological record that started approximately 250 kya and is associated with the appearance of the first fossil remains of modern humans, *Homo sapiens sapiens*. The first modern human forms appear about 190 kya in East Africa, which is in agreement with the estimation for the origin of modern humans based on population genetic studies. With the rise of modern humans in Africa, between 250 and 50 kya, bone tools began to be exploited, and spear heads and fishing appeared. Besides technological innovation, this period also witnessed the first appearance of unequivocal symbolic artefacts, such as pigment use by 160 kya and shell ornaments and cave engravings by 77 kya. Producing these artefacts involved a large number of steps, and maintaining such a culture demanded efficient systems of information transfer across generations. This cultural explosion was soon followed by successful colonization of other continents and could have accelerated the extinction of other hominid species. Strikingly, the now-extinct hominins that coexisted with *Homo sapiens* — including Neanderthals — do not appear to have produced symbolic artefacts, despite Neanderthals having a larger cranial capacity than *Homo sapiens*.

Relative Brain Size

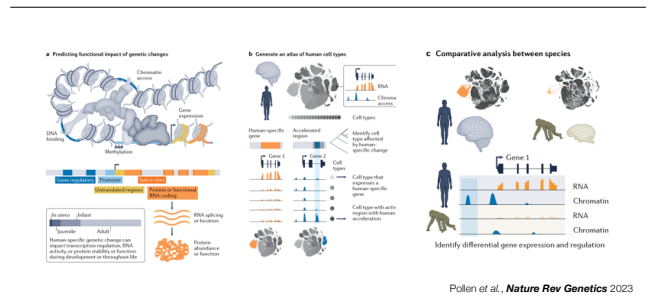


A comprehensive transcriptional map of primate brain development

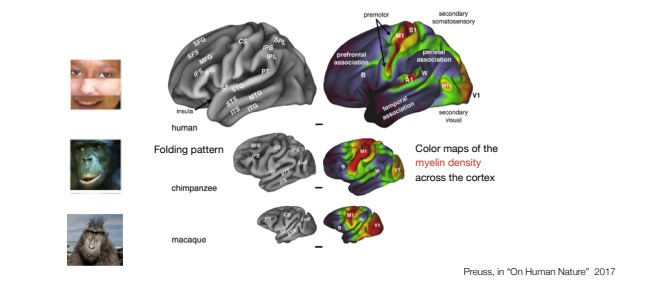


The transcriptional underpinnings of brain development remain poorly understood, particularly in humans and closely related non-human primates. We describe a high-resolution transcriptional atlas of rhesus monkey (*Macaca mulatta*) brain development that combines dense temporal sampling of prenatal and postnatal periods with fine anatomical division of cortical and subcortical regions associated with human neuropsychiatric disease. Gene expression changes more rapidly before birth, both in progenitor cells and maturing neurons. Cortical layers and areas acquire adult-like molecular profiles surprisingly late in postnatal development. Disparate cell populations exhibit distinct developmental timing of gene expression, but also unexpected synchrony of processes underlying neural circuit construction including cell projection and adhesion. Candidate risk genes for neurodevelopmental disorders including primary microcephaly, autism spectrum disorder, intellectual disability, and schizophrenia show disease-specific spatiotemporal enrichment within developing neocortex. Human developmental expression trajectories are more similar to monkey than rodent, although approximately 9% of genes show human-specific regulation with evidence for prolonged maturation or neoteny compared to monkey.

Single-cell genomic atlases to map and identify human-specific features

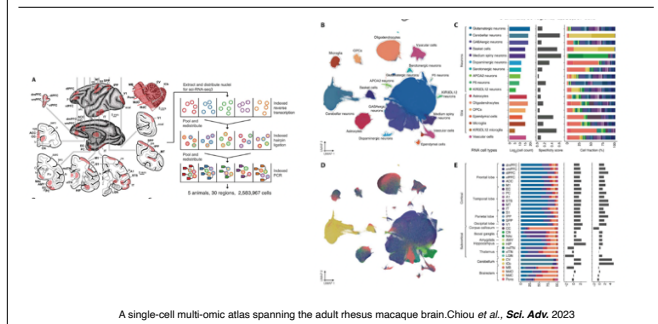


The major sulci, gyri, and functional divisions of the cortex in humans, chimpanzees, and macaques



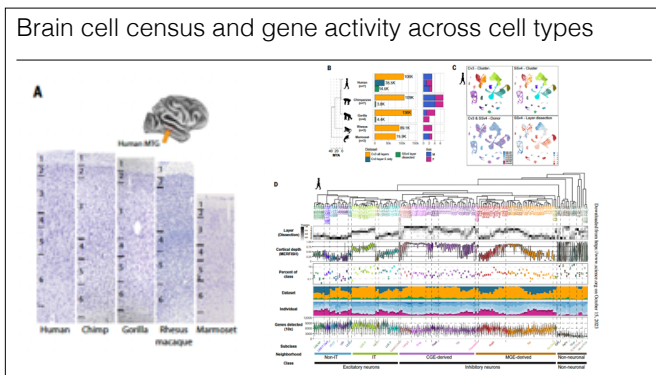
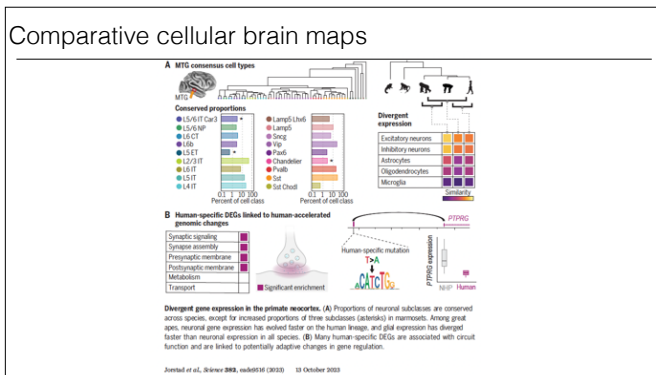
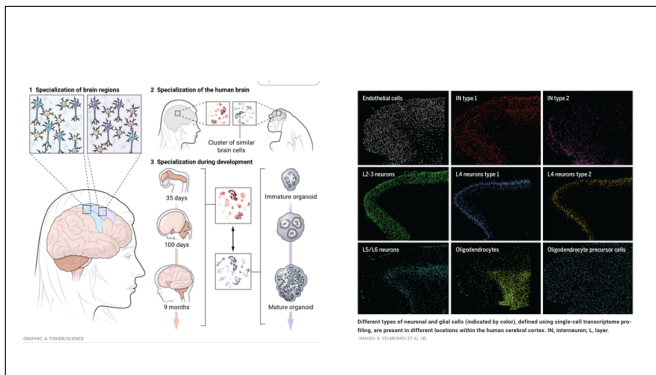
The major sulci, gyri, and functional divisions of the cortex in humans, chimpanzees, and macaques. These are lateral views of the left cerebral hemisphere drawn to scale. Figurines in the left panel illustrate similarities and differences in the folding patterns of the three species. Both chimpanzees and macaques possess a deep lunate sulcus (LuS), which separates primary visual cortex (V1) from secondary visual areas; humans lack an LuS. Also, macaque frontal lobes have a single longitudinal fissure, the principal sulcus (PS) rather than the two longitudinal fissures present in chimpanzees and humans, the inferior and superior frontal sulci (IFS, SFS). Figurines in the right panel display color maps of the myelin density across the cortex. The densely myelinated primary sensory areas visual (V1), somatosensory (S1), and auditory (A1) are red, as is the primary motor area (M1). The densely myelinated middle temporal visual region (MT?) is largely exposed on the surface in humans, but buried within the posterior part of STS in chimpanzees and macaques. The secondary sensory and premotor areas, somewhat less heavily myelinated, shade from red to green. The higher-order association regions are mainly blue. Association cortex makes up a much greater fraction of the cortical mantle in humans than in chimpanzees or macaques. Additional abbreviations: B, Broca's area; CS, central sulcus; IFG, inferior frontal gyrus; IP, inferior parietal lobule; IPS, intraparietal sulcus; ITG, inferior temporal gyrus; ITS, inferior temporal sulcus; MFG, middle frontal gyrus; MTG, middle temporal gyrus; MT?, the middle temporal visual complex; PT, planum temporale; SF, Sylvian fissure; SFG, superior frontal gyrus; SPL, superior parietal lobule; STG, superior temporal gyrus; STS, superior temporal sulcus; W, Wernicke's area. Images were captured from the Human Connectome Project (HCP) datasets using HCP Workbench software; the chimpanzee and macaque data are from scans collected at the Yerkes National Primate Research Center, processed through HCP pipelines. Scale bar is 1 cm.

Macaque brain, single cell sequencing of mRNA



Experimental setup and summary of the Macaque Brain Atlas snRNA-seq dataset. (A) Schematic of biopsied brain regions for sci-RNA-seq3 experiment. A full list of sampled regions is provided in table S1. arc, arcuate sulcus; cgs, cingulate sulcus; cs, central sulcus; ecal, external calcarine sulcus; iarc, inferior arcuate sulcus; ic, internal capsule; ips, intraparietal sulcus; ls, lateral sulcus; lv, lateral ventricle; p, principal sulcus; rf, rhinal fissure; sarc, superior arcuate sulcus. (B) UMAP visualization of all snRNA-seq profiled cells colored by cell type [with color code shown in (C)]. (C) Barplots showing the log₂-transformed cell counts (left), regional specificity score (middle), and regional composition [right, with color code shown in (E)] of each cell type. (D) UMAP visualization of all snRNA-seq cells colored by cell type [with color code shown in (E)]. (E) Barplots showing the cell type composition [left, with color code shown in (C)], log₂-transformed ratio of glutamatergic neurons and GABAergic neurons (middle), and log₂-transformed ratio of neurons and glial cells (right) of each region. Regions are organized by the regional subclass to which they belong.





Transcriptomic cell-type taxonomies of human and NHP MTG.

(A) Representative Nissl-stained cross sections of MTG in the five species profiled. The inset shows the approximate MTG region dissected from human brain.

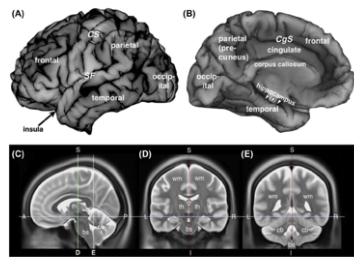
(B) Phylogeny of species (left; MYA, millions of years ago) and bar plots of nuclei that passed quality control (center) and sampled individuals (right) for each dataset.

(C) Uniform manifold approximation and projection (UMAP) plots of single nuclei from human MTG integrated across individuals and RNA-seq technologies and colored by cluster, individual ID, and dissected layer.

(D) From

top to bottom are the following: a human taxonomy dendrogram based on Cv3 cluster median expression; a heatmap of laminar distributions estimated from SSv4 layer dissections; violin plots of the relative cortical depth (pia to white matter) of cells grouped by type based on in situ measurement of marker expression in human MTG; a dot plot of cell-type abundance represented as a proportion of class (excitatory, inhibitory, glia), where error bars denote standard deviation across Cv3 individuals (L5 is the only dissection excluded); bar plots indicating the proportion of each cluster that is composed of Cv3 all layers, Cv3 layer 5 only, and SSv4 layer dissected datasets; bar plots indicating the proportion of each cluster that is composed of each individual; and violin plots showing the number of distinct genes detected from Cv3 datasets.

Human brain morphology

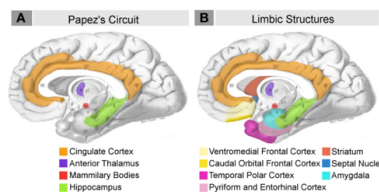


Preuss, in "On Human Nature" 2017

Human brain morphology. (A, B) The location of the major lobes are shown in lateral (A) and medial (B) views of the left cerebral hemisphere. The central sulcus (CS) separates the frontal and parietal lobes; the Sylvian fissure (SF) separates the temporal lobe from the frontal and parietal lobes. The insula is a region of limbic cortex buried within the SF. The cingulate sulcus (CgS) separates the cingulate cortex from the frontal and parietal cortex. (C-E) T2-weighted MRI images showing the relationship of the cerebral hemispheres to deep structures, including the thalamus (th), cerebellum (cb), and brainstem (bs). The section in C is in a parasagittal plane, with anterior (A) to the left. D and E are coronal sections; their locations are marked in C. In T2-weighted images, the cortical gray matter appears as a light rim surrounding the darker white matter (wm). Images were captured from the Human Connectome Project (HCP) datasets using HCP Workbench software. Additional abbreviations: I, inferior; L, left; P, posterior; R, right.

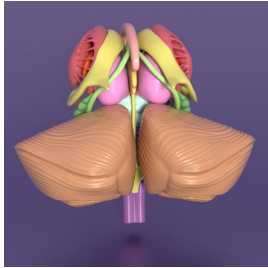
Under the Hood?

neural systems proposed to process emotion



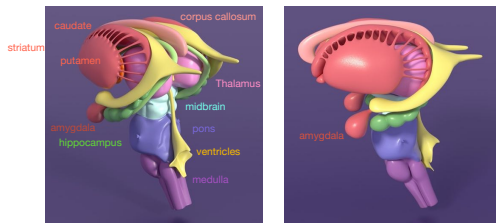
Schematic briefly summarizing neural systems proposed to process emotion, highlighting structures that are visible on the medial surface of the brain. Papez's (1937) original circuit (A) was expanded upon in the concept of the limbic system (B) to include a variety of subcortical and cortical territories (MacLean, 1952; Heimer and VanHoesen, 2006). (Structures like the anterior insula and nucleus basalis of Meynert, which are not visible on the medial surface of the brain, are not represented here). Images modified from Papez's (1937) original drawing.

Subcortical brain structures



<https://www.turbosquid.com/3d-models/3d-obj-realistic-subcortical-structures-human-brain/818190>

Subcortical brain structures



<https://www.turbosquid.com/3d-models/3d-obj-realistic-subcortical-structures-human-brain/818190>

- 1.) brainstem (medulla + pons), midbrain, thalamus, hypothalamus, pituitary gland and optic chiasm
- 2.) striatum (caudate-putamen and nucleus accumbens), amygdala
- 3.) nucleus pallidus
- 4.) hippocampus
- 5.) fornix with mammillary bodies
- 6.) corpus callosum
- 7.) ventricles
- 8.) cerebellum

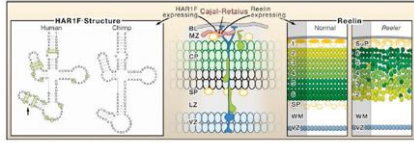
Subcortical brain structures



<https://www.turbosquid.com/3d-models/3d-obj-realistic-subcortical-structures-human-brain/818190>

Human accelerated region 1

HAR 1 encodes a functional RNA!



18/118 human specific changes to an RNA coding region

over 700 nCHARs!

expression during fetal brain development in cortex

Pollard et al. *NATURE* 2006
Haussler Group UC Santa Cruz

HAR1A is active in the developing human brain between the 7th and 18th gestational weeks.

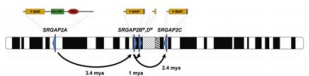
Cajal Retzius cell in marginal zone (MZ) stained with Golgi stain

20q13.33 of the HAR1-associated transcripts HAR1F and HAR1R, these micro RNAs associate with the protein Reelin, which is involved in fetal cortex organization.

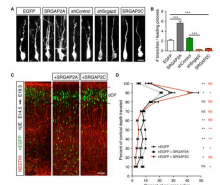
HAR1A is active in the developing human brain between the 7th and 18th gestational weeks. It is found in the dorsal telencephalon in fetuses. In adult humans, it is found throughout the cerebellum and forebrain; it is also found in the testes.

There is evidence that HAR1 is repressed by REST in individuals with Huntington's disease, perhaps contributing to the neurodegeneration associated with the disease.

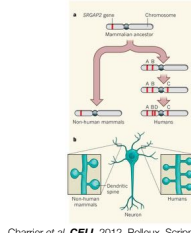
Evolution of human-specific neural SRGAP2 genes by incomplete segmental duplication



Dennis et al. *CELL* 2012,
Eichler Group UW



increased density of longer neuronal spines in transgenic mouse!

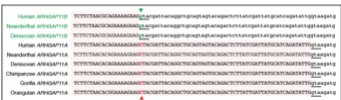


Charrier et al. *CELL* 2012, Polteux, Scripps

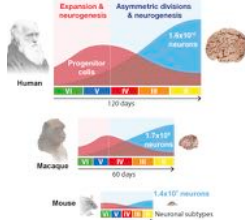
SLIT-ROBO Rho GTPase-activating protein 2 (srGAP2) also known as formin-binding protein 2 (FNBP2) is a protein that in humans is encoded by the SRGAP2. Schematic depicts location and orientation (blue triangles) of SRGAP2 paralogs on human chromosome 1 with putative protein products indicated above each based on cDNA sequencing. Asterisks indicate a 49 amino acid truncation of the F-BAR domain. Note that the orientation of SRGAP2D remains uncertain, as the contig containing this paralog has not yet been anchored. Arrows trace the evolutionary history of SRGAP2 duplication events. Copy number polymorphism and expression analyses suggest both paralogs at 1q21.1 (SRGAP2B and SRGAP2D) are pseudogenes, whereas the 1q32.1 (SRGAP2A) and 1p12 (SRGAP2C) paralogs are likely to encode functional proteins.

SRGAP2C Expression in Radially Migrating Mouse Cortical Neurons Phenocopies Srgap2 Knockdown (A) Confocal images of optically isolated neurons showing representative morphologies of radially migrating cortical neurons in E18.5 embryos following in utero electroporation (IUE) at E14.5 of the indicated constructs. sh, short hairpin. Scale bar, 10 μm. (B) Mean number of branches (±SEM) of the leading process of neurons as represented in (A). n = 3 animals/condition, 100–150 neurons/condition. (C) Low magnification confocal images of E18.5 cortical slices showing migration of in utero electroporated neurons expressing nuclear-EGFP (nEGFP) alone or together with SRGAP2A or SRGAP2C. Staining with anti-GFP shows the position of the electroporated neurons, and anti-NESTIN marks the radial glial scaffold. dCP, dense Cortical Plate. (D) Quantification of neuron distribution in cortical slices as illustrated in (C) (mean ±SEM). n = 3 animals/condition, 9–10 slices/condition. In (B) and (D), *p < 0.05; **p < 0.01; ***p < 0.001; NS (not significant, p > 0.05); Mann-Whitney test.

ARHGAP11B, incomplete duplication + splice site

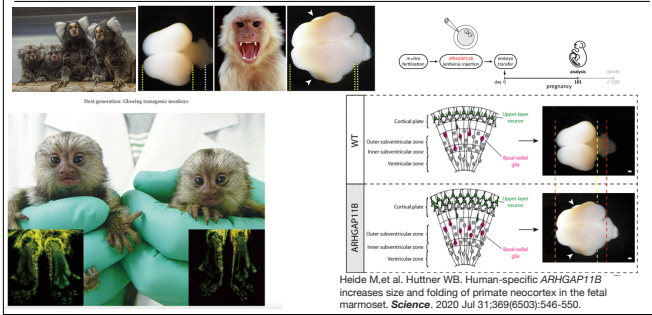


Alignment of modern human, Neanderthal and Denisovan ARHGAP11B and ARHGAP11A sequences with chimpanzee, gorilla and orangutan ARHGAP11A ortholog sequences



Reconstruction of the ancestral splice donor site. Alignment of modern human, Neanderthal and Denisovan ARHGAP11B and ARHGAP11A ortholog sequences. The boundaries between exons 5 (pink rectangles) and introns 5 are shown. Arrowheads indicate the C-to-G nucleotide substitution (red-to-green) in exons 5. Notice that the 'G' is only found in archaic and modern human ARHGAP11B. Exonic and intronic nucleotide sequences are displayed in upper and lower cases, respectively. Horizontal lines indicate splice donor sites.

Primate Models: Critique of Pure Marmoset

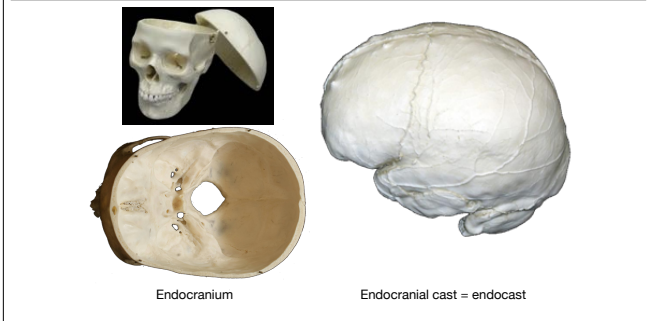


Marmosets, *Callithrix jacchus*, the model animals for primate neuroscience.

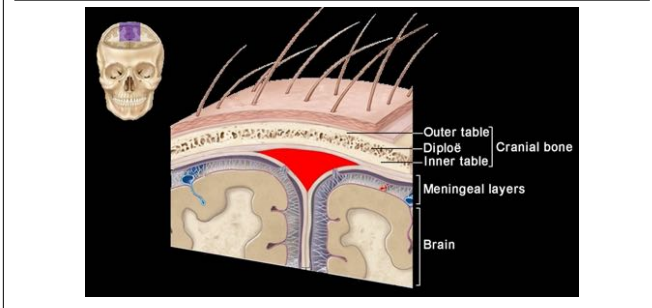
A critique of pure marmoset

<https://pubmed.ncbi.nlm.nih.gov/31416070/>

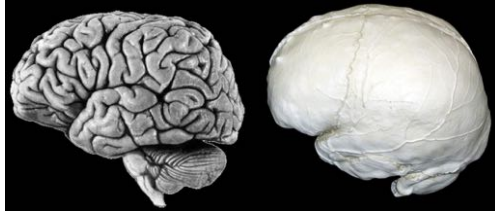
Endocast = cast of the inside of the braincase



Between the brain and the bone: the meninges



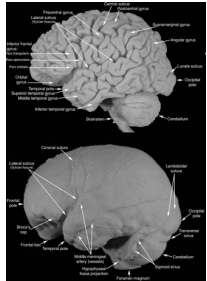
Endocast \neq brain



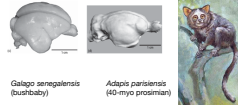
Brain

Endocast

Endocast and Brain Surface



Holloway et al., 2009



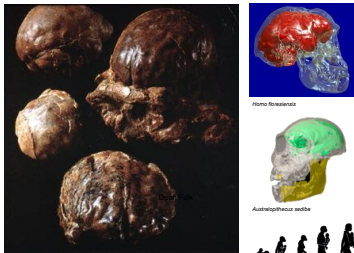
Galago senegaltensis
(posible baby)

Adapis parisiensis
(40 mya primate)

H. Jerison

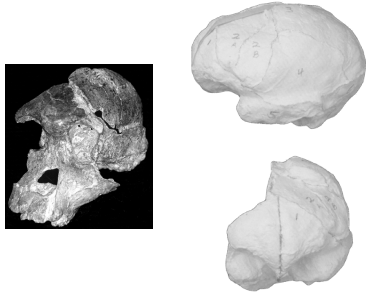
- Overall Brain/Endocranial Volume
- Relative Size/Shape of Lobes
- Convolution Pattern
- Asymmetry
- Blood Supply Patterns

Paleoneurology

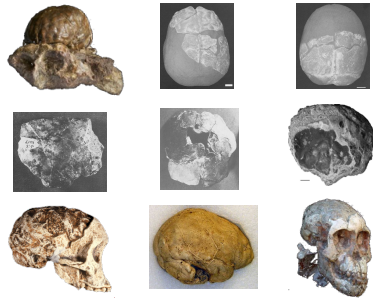


Endocrania (F. Holloway,
D. Falk, H. Jerison)

The artificial « physical » endocasts



The natural endocasts



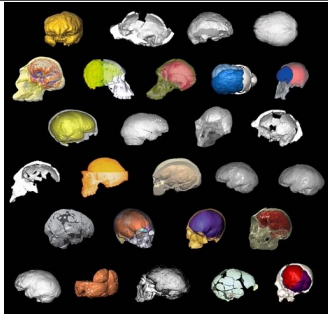
9 natural endocasts of fossil hominins

Australopithecus afarensis child



Famous skull with brain endocast of 3my old A afarensis child Selam (Dikika)

The artificial virtual endocasts from Thibault Bienvenu



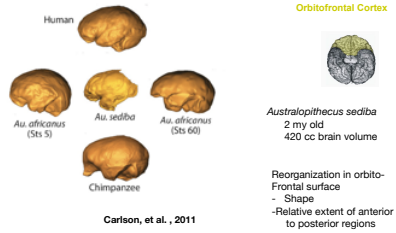
Thibault Bienvenu

27 virtual endocasts of fossil hominins

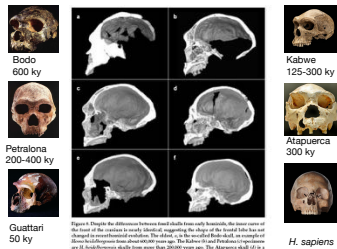
Australopithecine Endocasts

Some australopithecine endocasts have distinct features in the frontal and temporal lobes that place them closer to humans than to apes or other extinct hominids

Falk, 2011



The Fossil Record

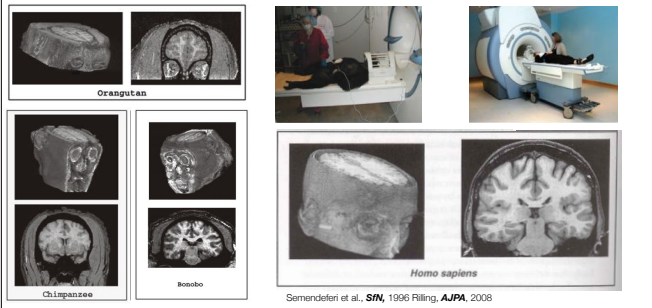


Despite differences btwn fossil skulls from early hominins, the inner curve of the front of the cranium is nearly identical.

→ Shape of the anterior frontal lobe has not changed in recent evolution.

(Bookstein et al., 1999)

Imaging Techniques (MRI)



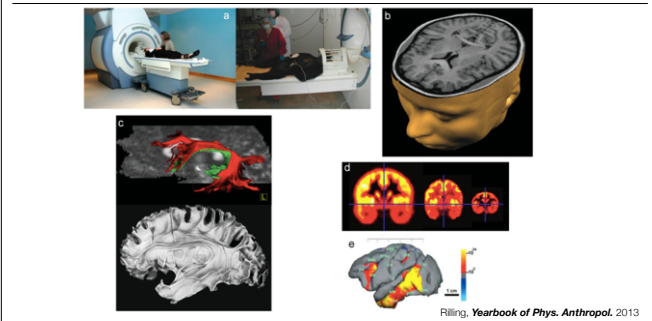
Imaging techniques

Technique	Example	Purpose	Advantages	Disadvantages
MRI Magnetic Resonance Imaging		Anatomical image of gray matter, white matter, and CSF	Can be conducted on anesthetized subjects	Microscopic (cellular) features not visible
DTI Diffusion Tensor Imaging		Reconstruction of white matter fiber tracts - imaging anatomical connectivity	Can be conducted on anesthetized subjects	Cannot track individual axons because of limited spatial resolution, cannot discriminate origins from termination of pathways
PET Positron Emission Tomography		Imaging brain function (glucose metabolism or blood flow) and receptor density and distribution	¹⁸ F-FDG PET enables functional imaging without restraint, fluorodeoxyglucose F-18 radiopharmaceutical emitting positrons.	Limited temporal resolution (on the order of minutes), involves the administration of radioactive tracers, ¹⁸ O water PET requires immobilization of awake animals, dependent on access to cyclotron
fMRI functional Magnetic Resonance Imaging		Imaging brain function (blood flow)	Good temporal resolution (seconds), tracer administration not required	Load, confining environment, requires immobilization of awake animals

Rilling, *Yearbook of Phys. Anthropol.* 2013

Different imaging techniques each come with their own advantages and limitations.

Imaging techniques: structural and functional



Structural neuroimaging.

- (a) MRI scanner with human (left) and chimpanzee (right) subject,
 (b) (b) axial section through human T1-weighted MRI scan,
 (c) DTI-based reconstruction of the human arcuate fasciculus pathway (top) and postmortem equivalent (bottom),
 (d) 18F-FDG PET images from human (left), chimpanzee (middle), and rhesus macaque (right), brighter colors (yellow to white) indicate higher levels of radioactivity and glucose metabolism.
 (e) fMRI activations related to object processing in awake rhesus macaque. Colored areas are more active when processing intact compared with scrambled objects. Activation is particularly strong in the ventral temporal cortex, the presumed location of the macaque object recognition or “what” pathway. [(a) Left, from: http://www.epilepsyse.org.uk/media/pics/piclibrary/3T2_high.jpg; right, personal photograph. (e)

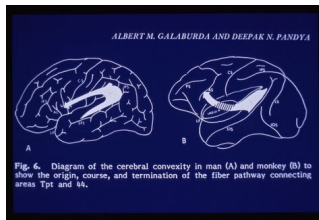
Arcuate Fasciculus



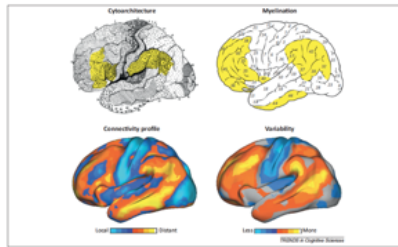
An arching bundle of association fibers through the frontal, parietal, and temporal lobes.

Connects Broca's and Wernicke's areas.

Involved in special language related conditions:
e.g. Conduction Aphasia:
Inappropriate responses to heard communication



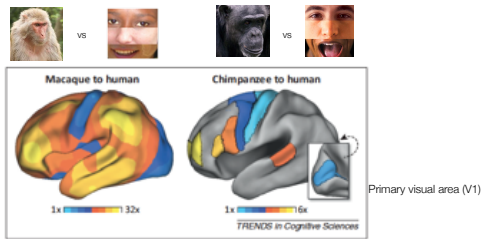
Distributed association networks



Buckner and Krienen Trends in Cog Sci, 2013

Association cortex matures late and possesses functional properties that are different from sensory regions. Top: Brodmann's (1909) cytoarchitectonic map and Fleschig's (1920) developmental myelination estimates are displayed [28,79]. Numbers for cytoarchitecture arbitrarily label the distinct zones of cortex and have come to be known as Brodmann areas. Regions shaded in yellow are frontal and parietal areas that Brodmann (1909) proposed had no monkey homologs. Myelination numbers designate the relative ordering of developmental myelination, with higher numbers indicating late development. The regions shaded in yellow mature late. Bottom: Functional MRI estimates of organizational properties. Distant connectivity quantifies the relative percentage of strong functional correlations that are distant from the region (e.g., across lobes) versus local correlations. Warmer colors reflect regions that have preferentially long-range functional connectivity. Variability displays regions with the greatest between-subject variation in functional organization estimated by functional connectivity.

Expansion of distributed association zones



Estimates of cortical expansion

Buckner and Krienen *Trends in Cog Sci.* 2013

Distributed association zones are disproportionately expanded in humans. Estimated cortical expansion is illustrated for macaque to human and for chimpanzee to human. Colors represent the scaling value required to achieve the size in the human brain. The data are projected onto the left hemisphere cortical surface of the population-average, landmark- and surface-based atlas. For the macaque, a continuous surface estimate of expansion is computed from 23 distributed landmarks. For the chimpanzee expansion plot, area estimates for a limited set of discrete areas are presented from Table 2 in [6]. The primary visual area (V1) is displayed in the inset.

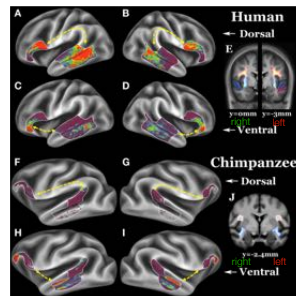
Where language happens?

Dorsal derived versus ventral conserved.

Arcuate fasciculus is massively developed on the left side in humans

Evidence for both, Continuity and Divergence

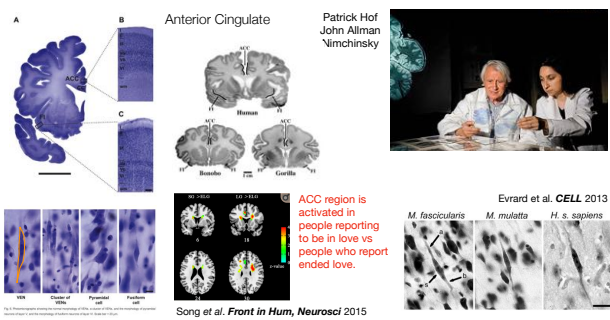
Diffusor Tensor imaging, group average of 26 humans and 26 chimpanzees



Rilling et al. *Front. in Neurosc.* 2012

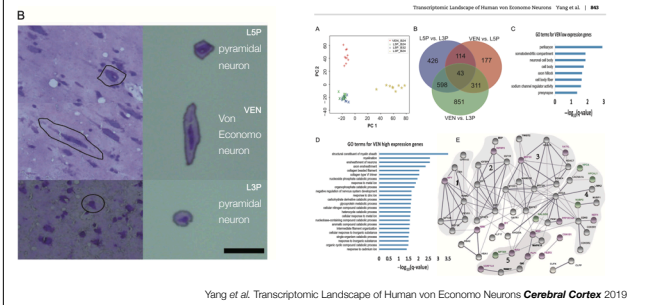
Comparative DT data suggest that the specialized, derived features of human language (syntax and lexical-semantic) are likely to be mediated by the arcuate fasciculus pathway.

Von Economo Neurons (elusive spindle neurons)



Large comical neurons with particular shapes: VEN Von Economy Neurons

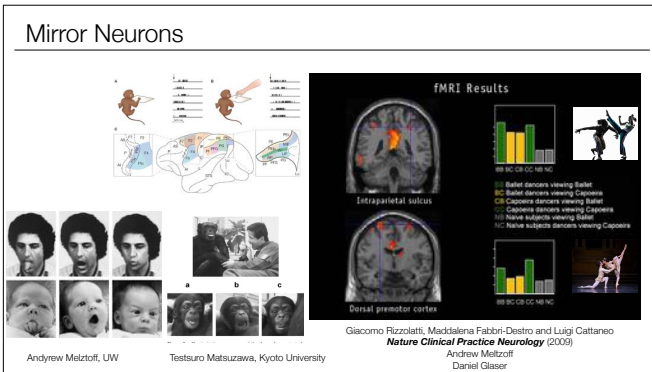
Transcriptomic Landscape of von Economo Neurons



Transcriptome comparison among VENs, L5Ps, and L3Ps, and functional enrichment and protein-protein interaction (PPI) analyses of VEN-associated differentially expressed genes (VA-DEGs).

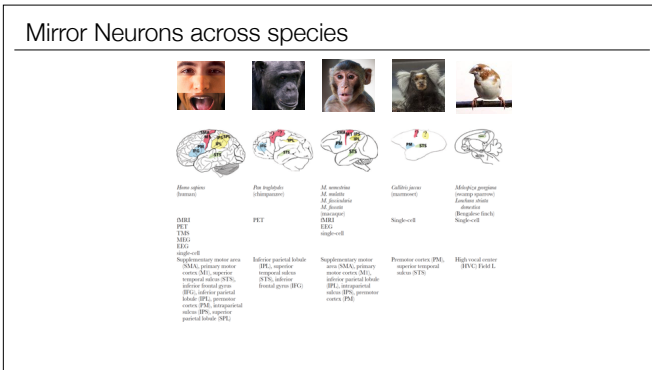
- The **adjustment for confounding variation principle component analysis** (AC-PCA) map showing clustering of VENs and pyramidal neurons (L5Ps and L3Ps);
- Counts of cell-type-specific genes with expression changes;
- Functional enrichment** of the 129 lower expression VA-DEGs;
- Functional enrichment of the 215 higher expression VA-DEGs;
- The **protein-protein interactions (PPI)** network with five clusters of genes associated with VEN morphology and functions. The five PPI clusters were classified based on the local PPI patterns and functional relatedness of the genes. The purple circles are the high expression VA-DEGs, and the green circles are the low expression VA-DEGs. The gray circles are genes

Mirror Neurons, how do they look, what is their biochemical signature? No molecular markers.....

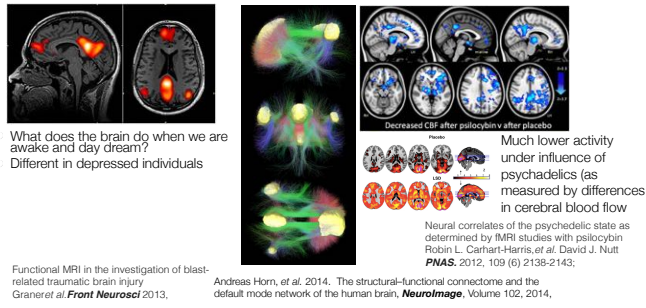


The brains of human, chimpanzee, macaque, marmoset and songbirds with the cerebral locations where mirror neurons have been investigated and found. On the brain images these are highlighted in red (motor areas), yellow (parietal areas), blue (premotor areas) and green (sensorial areas). For each species, the techniques used to record mirror neuron activity are specified.

- fMRI, functional magnetic resonance;
- EEG, electroencephalography;
- TMS, transcranial magnetic stimulation;
- PET, positron emission tomography;
- MEG, magnetoencephalography

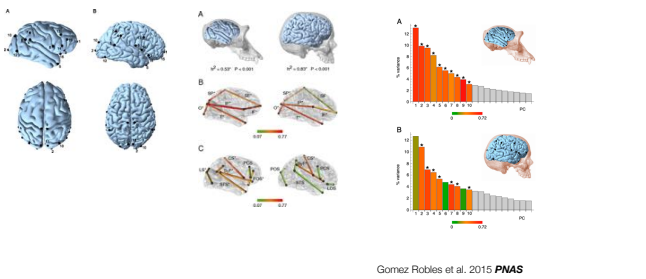


Brain Default Mode Network?



This network is strongly inhibited by LSD and Psilocibin and the inhibition is associated with self reports of “ego-dissolving” sensation. This begs the question about who is watching the “ego” dissolve.

Relaxed genetic control of cortical organization in human brains compared with chimpanzees



The authors used mother-offspring, full-sib, half-sib and monozygotic twin comparisons to calculate heritabilities of brain morphology variation.

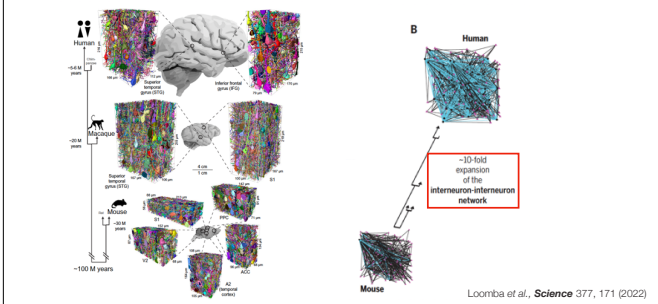
Heritability for brain size and lobe dimensions. (A) Heritability for brain size (brain volume including white and gray matter but not ventricular spaces) for chimpanzees (Left) and humans (Right). (B) Heritability for cerebral lobe dimensions in chimpanzees (Left) and humans (Right). IF, inferior frontal length; IP, inferior parietal length; O, occipital length; SF, superior frontal length; SP, superior parietal length; T, temporal length. (C) Heritability for sulcal lengths in chimpanzees (Left) and humans (Right). CS, central sulcus; FOS, fronto-orbital sulcus; LOS, latero-orbital sulcus; LS, lunate sulcus; PCS, precentral sulcus; POS, parieto-occipital sulcus; STS, superior temporal sulcus; SyF, Sylvian fissure. In B and C lobe dimensions and sulci are color-coded according to heritability values as indicated in the color scale bars. Lobe dimensions and sulci marked with an asterisk show significant heritability after a false-discovery rate approach was used to control for multiple comparisons. Detailed heritabilities, SEs, and P values are listed in Tables S3 and S4. In B and C chimpanzee and human brains are not to scale. Boxplots showing variation in linear metrics. Data for chimpanzees (c) are shown in yellow, and data for humans (h) are shown in blue. (A) Variation in original lobe dimensions (in native space). (B) Variation in original sulcal dimensions. In A and B dimensions are provided in millimeters. (C) Variation in lobe dimensions measured in Procrustes-superimposed configurations of landmarks. (D) Variation in sulcal dimensions in Procrustes-superimposed configurations. In C and D linear dimensions were measured after scaling all individuals to a centroid size of 1. In A and C, IF, inferior frontal length; IP, inferior parietal length; O, occipital length; SF, superior frontal length; SP, superior parietal length; T, temporal length. In B and D, CS, central sulcus; FOS, fronto-orbital sulcus; LOS, latero-orbital sulcus; LS, lunate sulcus; PCS, precentral sulcus; POS, parieto-occipital sulcus; STS, superior temporal sulcus; SyF, Sylvian fissure. Anatomically homologous landmarks used in this study. (A) Anatomically homologous landmarks in chimpanzee brains in lateral view (Upper) and dorsal view (Lower). (B) Anatomically homologous landmarks in a representative human brain in lateral view (Upper) and dorsal view (Lower).

Right: Distribution of variance and heritability of phenotypic shape variation.

(A) Scree plot showing the distribution of shape variance in chimpanzee brains.

(B) Scree plot corresponding to shape variation in human brains. Heritabilities for the first 10 PCs are represented using a color code. PCs marked with an asterisk show significant heritability after a false-discovery rate was applied to control for multiple comparisons. Only the first 20 PCs are represented; heritabilities of PC11–PC20 have not been estimated because they account for very minor proportions of variance.

Comparison of mouse, macaque, and human connectomic datasets from the cerebral cortex

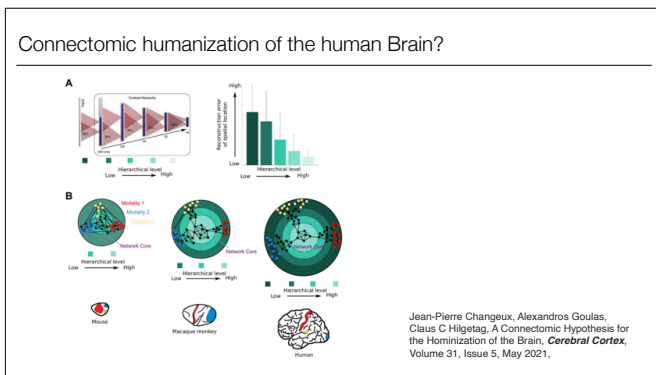


Connectomic screening across mammalian species: Comparison of five mouse, two macaque, and two human connectomic datasets from the cerebral cortex.

(A) Comparative connectomic analysis of mouse, macaque, and human cortex. Dense connectomic reconstructions from L2/3 of five cortical areas of mouse (bottom, $n = 5$ individuals) and from four cortical areas of macaque and human ($n = 3$ individuals). There are matched cortical areas (A2 and STG) across all three species and paired samples from S1 (mouse and macaque). A total of 202,954 axons and 1,618,129 synapses were analyzed (Materials and methods). The raw 3D EM data of mouse datasets S1, V2, PPC, and ACC were previously published (55), but their dense reconstruction have not. (Left) Simplified phylogenetic tree [based on (100)] indicating time to last common ancestor between human (*Homo sapiens*), rhesus macaque

(Macaca mulatta), and mouse (Mus musculus). Scale bars apply to the brain sketches. S1, primary somatosensory cortex; A2, secondary auditory cortex; V2, secondary visual cortex; PPC, posterior parietal cortex; ACC, anterior cingulate cortex; STG, superior temporal gyrus; IFG, inferior frontal gyrus.

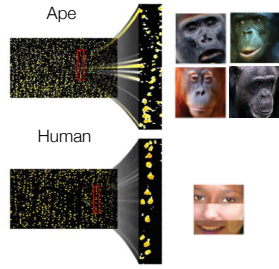
(B) Illustration of the about 10-fold expansion of the interneuron-to-interneuron network from mouse to human.



Evolution of the multilevel connectomic architecture for neural representations in biological and artificial brain networks. (A) Multilevel artificial neural network architecture (left). A synthetic agent with a multilevel visual system can navigate a natural environment. Activity in the artificial neural network in higher levels allows a more accurate reconstruction of the location of the artificial agent (right). Note the decrease of the error of location reconstruction with increased level. Thus, a serial, convergent processing of activity from the sensorium to higher levels of the network enables abstract representations. (B) Enlargement of the brain and expansion of the association cortex can lead to the overall sparsification of the network (cf. Fig. 1), and, in addition, to an expanded multilevel structure of the human brain. The increased number of levels, or processing stages, defined as synaptic steps between neurons, is due to the expansion of the association cortex in humans in relation to monkeys and presumably other primates. In humans, sensory areas drift apart in physical space and, thus, do not directly connect with each other, but integrate information through a multilevel connectomic architecture toward the network core. The presence of more hierarchical levels may bestow the human brain with increased capacity for more refined and abstract representations of the sensorium. (A) Modified from Wyss et al. (2006). Brains in (B) from Krubitzer and Seelke (2012). Modality: 1 = somatosensory; 2 = auditory; 3 = visual.

Density of neurons

Bigger brains:



More neurons
Decrease in density of neurons
Increase of cortical sheet horizontally
More vertical arrays/minicolumns
More cortical surface
Increased convolutions

Rakic, 1995

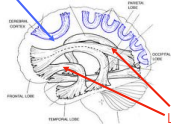
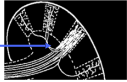
More space between neuronal bodies

D. Buxhoeveden
K. Zilles
H.B. Uylings

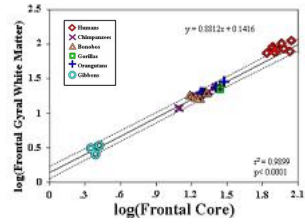
White Matter Distribution

Human brains have different distribution of white matter → increased local connectivity

Local Connections



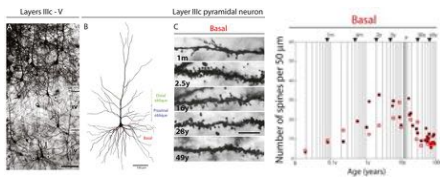
Long Distance Connections



Schenker et al., 2005

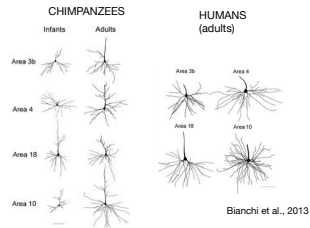
Branching Patterns

Branching of pyramidal neurons in the dorsolateral PFC increases during development in humans (and non human primates)



Petanjek et al., 2011

Dendritic Complexity



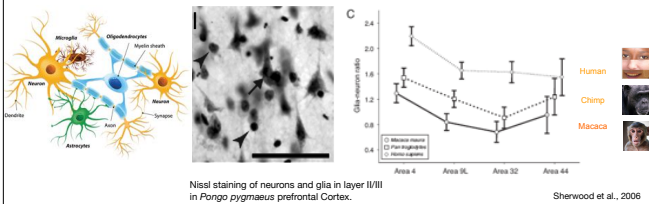
Chimps: Greater dendritic complexity in PFC than other areas.
Complexity increases in early development
Humans: Longer and more branched across areas

Chimps: Greater dendritic complexity in PFC than other areas. Complexity increases in early development
Humans: Longer and more branched across areas

Human frontal cortex has a higher ratio of glia to neurons

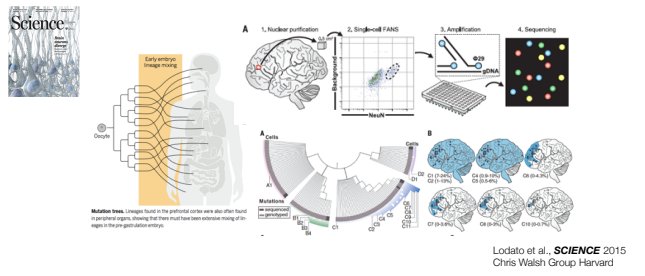
Glial cells regulate the rate of glucose uptake, and thus the flux of energy, to neurons.

Increased number of glia relates to energetic costs of maintaining larger dendritic arbors and long range projecting axons in the human brain.



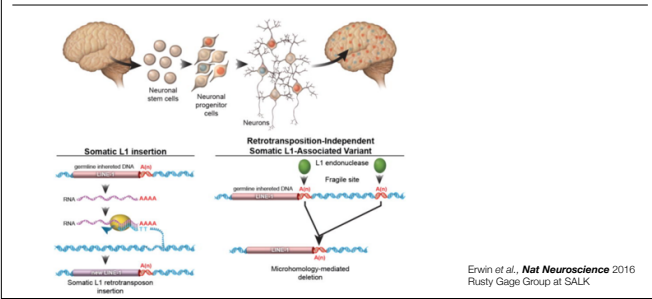
The ration of neuronal to glia cells differs.

Mutations in individual Neurons: Polyclonal Architecture!!



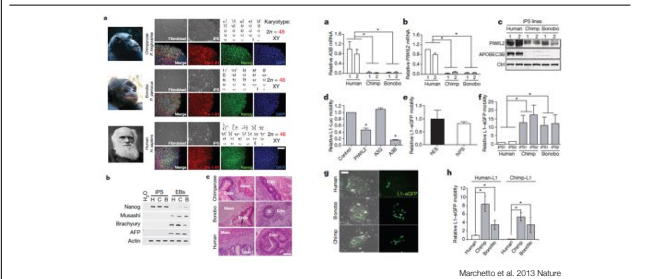
COVER Illustration of projection neurons from the human cerebral cortex, with nuclei colored to reflect distinct sets of somatic DNA mutations. When a mutation occurs in a dividing cell, it marks all of the cell's descendants. Identification of clones marked by mutation enables reconstruction of human brain development. Because developmental defects lie at the heart of many neurological diseases, understanding development is a primary goal of neuroscience.

Somatic L1 (retrotransposon)
Associated Variants



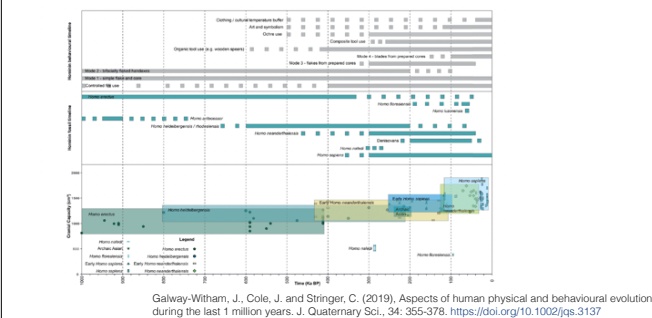
For somatic L1 insertions, a germline-inherited LINE-1 sequence is transcribed into RNA. The L1 endonuclease and reverse transcriptase protein nicks the genomic DNA and reverse transcribes the L1 RNA, resulting in the insertion of a new copy of Line-1 sequence. For retrotransposition-independent SLAVs, L1 endonuclease preferentially cuts a germline-inherited LINE-1 sequence and recombination with a downstream A microsatellite results in a microhomology-mediated deletion. The A microsatellite regions may be nicked by the L1 endonuclease or a fragile site within the genome of neural progenitor cell.

iPS Ape and human neurons
Apobec3 and L1 activity



Human neurons control retrotransposons more stringently than ape neurons (in a dish). Some human mental conditions e.g. Rett's syndrome, a severe form of autism in girls is associated with increased retrotransposon activity in neurons.

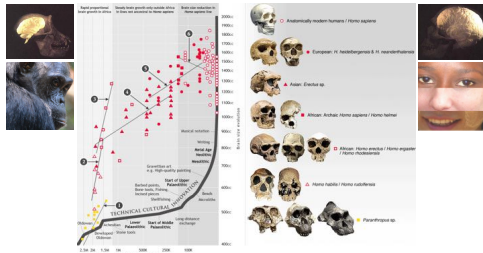
Behavior, Fossils, Cranial Capacity



Timeline illustrating key behavioral traits, hominin fossils and endocranial volume (data from S1) during the last million years. For the behavioral traits and fossils, the solid line represents more certain date ranges, while the segmented lines represent more ambiguous data points that extend beyond the range of established dates. The spacing of the horizontal segmented lines relates to the relative certainty of the associated dates. The fossil timeline does not include any phylogenetic inference. The coloured boxes represent endocranial volume ranges to illustrate areas of overlap in inferred brain size between taxa. Although we have used cited dates in relation to fossils, we do not necessarily agree with all of them.

Brain expansion over time

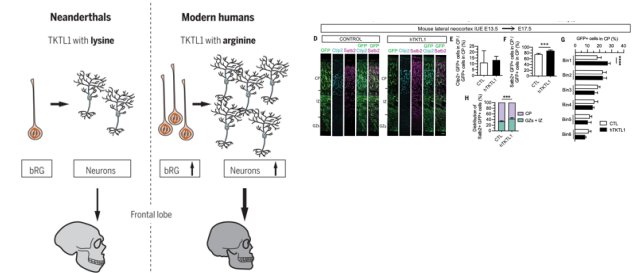
Driven by culture and/or driving culture?



Bradshaw Foundation adapted from Steven Oppenheimer, 2012 Out of Eden

How we went from an ancestor with a chimp-sized, 400 cc brain to a modern 1500cc brain and the technology accompanying, or driving? it.

TKTL1 gene and Hominid Cortical Neurogenesis

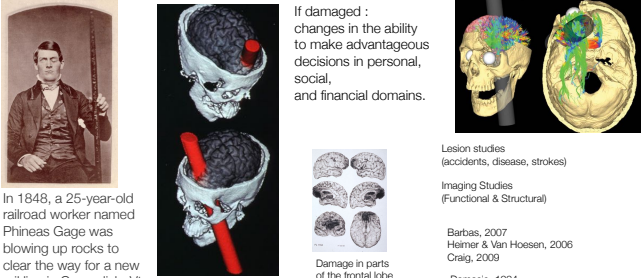


The single lysine-to- arginine substitution in modern human TKTL1 leads to greater bRG numbers than in Neanderthals. These bRG in turn generate more neocortical neurons in modern humans. Because TKTL1 expression in fetal human neocortex is particularly high in the developing frontal lobe, these findings imply that the frontal lobe of modern humans contains more neurons than that of Neanderthals.

Fig. 2. The hTKTL1-induced increase in bRG in embryonic mouse neocortex results in increased production of cortical neurons, notably upper-layer neurons, at late neurogenesis. (A to C) Modeling of the number of neurons generated, over 10 cell cycles, by the aRG → bIP → neuron lineage (A), the aRG → bRG → neuron lineage (B), or the aRG → bRG → neuron lineage with one round of hTKTL1-induced symmetric proliferative bRG division (C). Curved arrows denote self-renewal. (A) and (B) are adapted from figure S4 of (12). (D to H) Mouse neocortex E13.5 IUE with GFP plasmid, together with either empty (control, CTL) or hTKTL1 plasmid; analyses: E17.5. (E) to (H) are means of 5 embryos. Error bars, SD. (D) GFP/Ctip2/Satb2 (green/cyan/magenta) immunofluorescence. Scale bar, 30 μm. [(E) and (F)] Percentages of GFP+ cells in CP that are Ctip2+ (E) and Satb2+ (F). Unpaired Student's t test, (F) ***P < 0.001. (G) Percentages of the GFP+ cells in CP that are in bins 1 to 6 (bin 1, uppermost layer; bin 6, deepest layer) of CP. Two-way ANOVA with Bonferroni post hoc test,

****P < 0.0001. (H) Distribution of GFP+/Satb2+ cells in germinal zones (GZs) plus intermediate zone (IZ) versus CP. Student's t test, ***P < 0.001.

Impulse Control – Orbitofrontal & vmPFC



In 1848, a 25-year-old railroad worker named Phineas Gage was blowing up rocks to clear the way for a new rail line in Cavendish, Vt.

If damaged : changes in the ability to make advantageous decisions in personal, social, and financial domains.

Damage in parts of the frontal lobe in a human brain

Lesion studies (accidents, disease, strokes)








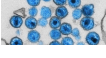
Imaging Studies (Functional & Structural)

Barbas, 2007
Heimer & Van Hoesen, 2006
Craig, 2009

Damasio, 1994
Bechara, 2010

Traumatic brain damage can be revealing.....work accident with tamping iron igniting an explosive charge, resulting in the iron rod shooting through Gage's skull.

Insults to brain development:

	Development	Adulthood
genetic accidents		
nutritional inadequacy		
emotional/social insults		
infection		

Causes of mental disease often combine genetic and environmental factors, both during development and adult life.

Practice question: Apart from genetic accidents, malnutrition, social insults and infection, what other factor can dramatically derail normal brain development?

Answer: Toxins such as lead paint or mercury poisoning, or alcohol poisoning via an alcoholic mother.

Over drugging the Mind?

Comfortably Numb HOW PSYCHIATRY IS MEDICATING A NATION



Charles Barber

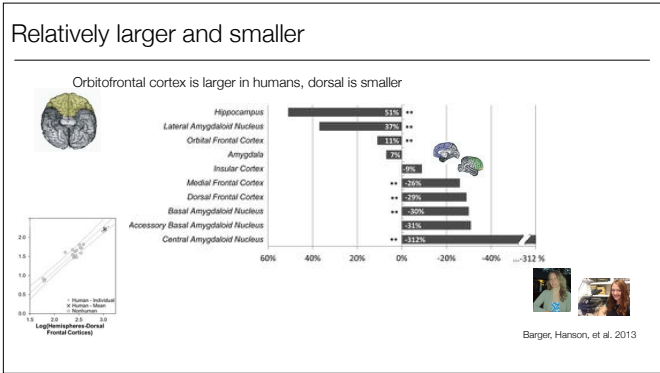
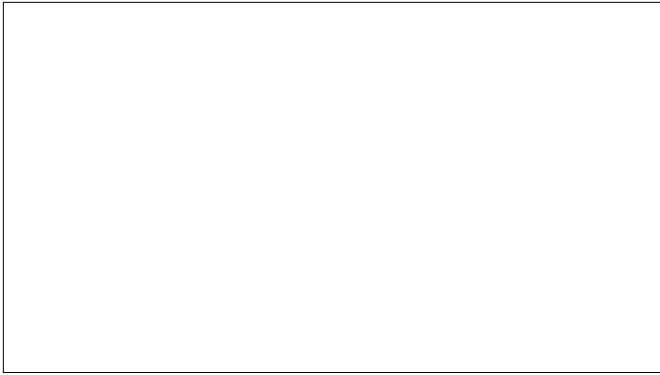
In 2006, the US, with 6% of the world's population, bought about 2/3 of the world's psychiatric drugs.

Practice question: What fraction of the world's psychiatric drugs are consumed by the US (6% of global population)?

Answer: 2/3!

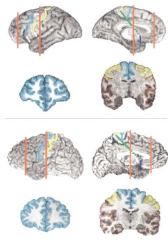
Summary Brain Evolution

- Brain changes range from the macro to the nano.
- Tripling of absolute brain size in the last 3 million years.
- Fossil endocasts and virtual endocasts shed some light on gross dimensions over that past 6 my.
- Imaging techniques allow comparative neuroanatomy in live hominids.
- Human brains grow for longer and at sustained rates in utero and after birth.
- Delayed maturation and expression of genes, synaptogenesis and myelination in humans.
- Human neocortex is not larger than expected for a primate our size.
- Connectivity has changed, e.g. intra-hemispheric is higher in humans, arcuate fasciculus is much expanded.
- Neuron morphology, numbers and distribution vary in several regions of the human brain.
- Subcortical areas especially the amygdala (social brain) has undergone human specific changes.
- Cell-type specific changes: VEN and mirror neurons?
- Novel genes and gene variants are involved even since the split from common ancestor with Neanderthals.

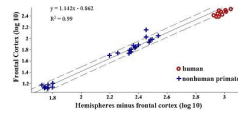


Human brains have expanded and shrunk certain areas in comparison to non-human primates.

Anatomically informed boundaries show that..

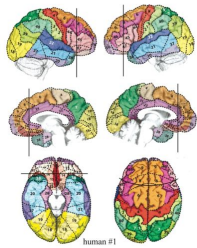


The human frontal cortex, both a) with and b) without the precentral gyrus (primary motor cortex) is as large as expected for an ape of human brain size



Semendefari et al., 1997; 2002

How to slice?

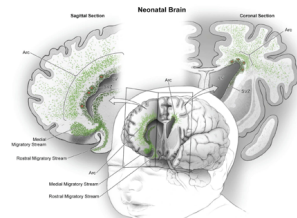


Stereotaxic planes are used with large samples of human brains in imaging.

Such planes cut through cortical territories
 → less informative for questions about volume of cortical regions (eg. frontal cortex or PFC).

Images courtesy of Hanna Damasio

Neuronal migrations in the neonatal brain



during first 7 months of life, neurons migrate into the anterior cingulate cortex

Paredes et al. *Science* 2016

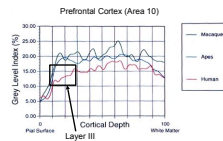
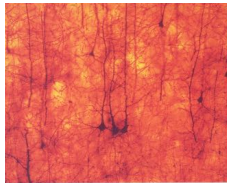
Neuropil: space around neurons

Human brains have decreased cell body density and more space available for connections.

Zilles et al., 1986

The human brain has differentially increased neuropil space in the layer III of PFC.

Semendeferi et al., 2001

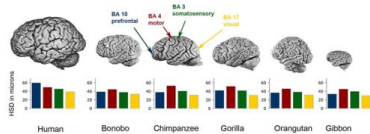


Neuropil is the amount of space around cell bodies available for connections (dendritic arbors, axons, glia, vasculature)

Spacing of cells

Spacing of the neurons and thus the size of minicolumns is NOT predicted by overall brain size.

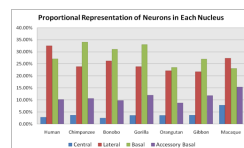
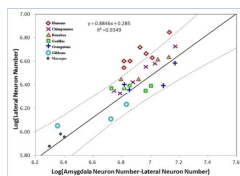
Spacing of neurons is NOT the same among cortical areas within each brain.



Humans have more space than apes between neuronal bodies in areas of the Prefrontal Cortex but not as much in other parts of the brain

Semendeferi/Teffet et al. *Cerebral Cortex* 2011

Neuron numbers in lateral nucleus of amygdala stand out in humans



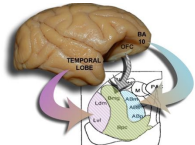
The amygdala has a unique organization in humans
The lateral nucleus is the largest component of the basolateral division in humans
Apes have the largest basal nucleus

Barger et al. JCN 2012



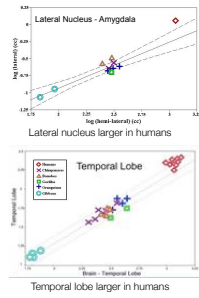
Evolutionary action in the social brain?

Lateral nucleus of Amygdala

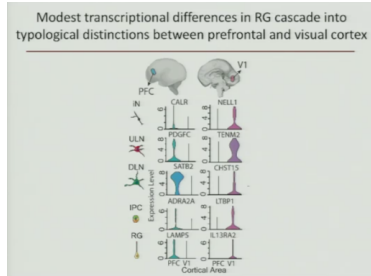


Lateral nucleus is highly interconnected with the temporal lobe.

Helen Barbas; Lisa Stefanacci
Semendeferi & Damasio, 2000
Rilling & Reiligman, 2001
Barger et al., 2007, 2012



Gene expression in individual cortical genes



Gene expression in radial glia can differ depending on region of the brain.
Radial glia cells disappear once the cortex is established!